Regular Article

PHYSICAL CHEMISTRY RESEARCH
Published by the
Iranian Chemical Society
www.physchemres.org
info@physchemres.org

Phys. Chem. Res., Vol. 8, No. 3, 373-397, September 2020
DOI: 10.22036/pcr.2020.213221.1712

Molecular Insight into the Mutual Interactions of Two Transmembrane Domains of Human Glycine Receptor (TM23-GlyR), with the Lipid Bilayers

F. Hamedi and D. Mohammad-Aghaie*

Department of Chemistry, Shiraz University of Technology, Shiraz 71555-313, Iran

(Received 25 December 2019, Accepted 23 March 2020)

Appearing as a computational microscope, molecular dynamics (MD) simulation can 'zoom in' to atomic resolution to assess detailed interactions of a membrane protein with its surrounding lipids, which play important roles in the stability and function of such proteins. This study has employed the MD simulations to determine the effect of added DMPC or DMTAP molecules on the structure of DPPC bilayer, and also to characterize the mutual interactions of TM23-GlyR (the second and third transmembrane domains of glycine receptor) with the pure and mixed lipid bilayers. Structural properties of DPPC bilayer, namely the order of acyl chains and the area per lipid, were affected by cationic DMTAP and zwitterionic DMPC lipids, in completely reverse ways. In the case of the mutual interactions between lipid molecules and TM23-GlyR, the cationic DMTAP lipids showed greater impact on the structural properties of this protein. On the other hand, TM23-GlyR caused clear increase in the lipid chain order, due to the positive hydrophobic mismatch. This study could shed light on the effect of lipid force field, chain length, and the head group charge and size on the lipid-protein interplay.

Keywords: Glycin receptor, DPPC, DMPC, DMTAP, Lipid-protein interactions, Molecular dynamics simulation

INTRODUCTION

The inhibitory glycine receptor (GlyR) is a membrane protein mediating fast synaptic transmission in the central nervous system (CNS), predominantly the spinal cord and the brain stem [1,2]. As a member of nicotinic acetylcholine receptor family of ligand-gated ion channels, GlyR is comprised of 4α and 1β sub-units, surrounding a central pore, which constitute a permeable channel to the chloride ions [3]. Each subunit of this receptor is composed of four α-helical transmembrane segments (TM1-TM4), along with a ligand-binding extracellular domain (ECD) [4].

Glycine, the smallest and simplest aminoacid, is the ligand for glycine receptor and operates as an inhibitory neurotransmitter in the central nervous system. In response to the neurotransmitter binding to its site on the external receptor surface, the GlyR transiently opens its Cl^--selective pore, in order to facilitate the passive diffuse of chloride ions, down their electrochemical gradient, through the lipid membrane. This ion flux changes the potential across the membrane and decreases the neuron capability to transmit signals to other neurons, *via* affecting the opening probability of voltage-gated channels [5-8].

GlyR, as other membrane proteins, spends its time surrounded by a shell of lipid molecules, equivalent to the solvent layer surrounding a water-soluble protein. For a long time, researchers thought that lipids were just a backdrop for the real players, while recent studies have revealed their important roles in regulating the structure, function, and dynamics of membrane proteins [9]. Today's picture, considers biological membranes as dynamic structures that vary in their lipid, protein and carbohydrate composition, coevolving and operating together [10].

It is known already that several aspects of the cell membrane influence the function of membrane proteins: The thickness, and phase of the lipid bilayer, as well as the

*Corresponding author. E-mail: d_aghaie@sutech.ac.ir

presence of certain phospholipids [11]. The lipid membrane environment influences the conformational space, explored by the peptide [12]. Specific lipid-protein interactions, contributing to the anchoring and stabilization of integrated membrane proteins, play an important role in a large number of crucial processes, occurring at the surface of the cell [13].

It is energetically convenient for a membrane protein to correspond its hydrophobic domain length with the hydrophobic thickness of the lipid bilayer. In case of existing hydrophobic mismatch, the peptide-lipid system undergoes compensatory alterations to alleviate the energetically unfavorable mismatch in lengths [14].

Although experimental methods such as X-ray and neutron scatterings [15,16], infrared (IR) spectroscopy [17] and solid state nuclear magnetic resonance (NMR) [18] provide useful information regarding the peptide-lipid interactions, little knowledge is available concerning their microscopic nature.

In the absence of detailed structural and biophysical/biochemical characterization of protein/lipid interactions, molecular dynamics (MD) simulations are able to provide a key tool, for probing the interactions of lipids with membrane proteins. In fact, simulations analyze the molecular level interactions between single molecules, providing complementary information to experiments [19]. So, even qualitative information gained by performing computer simulations of protein-membrane complexes are valuable.

Systematic investigation of complex membrane-protein interactions requires the simplified model membranes and peptides to reduce the computational cost. The model lipid membranes are often comprised of only one or two lipid species, while the model proteins are typically single α-helical peptides, with a large central hydrophobic region, and flanking polar or charged residues [14,20-21].

We have previously studied the phase behavior of DPPC monolayers at the water-air interface, through the atomistic molecular dynamics simulations. Reported pressure-area isotherms in the interval of 273-310 K confirmed the liquid condensed (LC) to liquid expanded (LE) phase transition, indicating that ordered condensed phase can nucleate from a starting disordered phase, on a time scale of approximately 50 ns [22]. In a more recent study, we investigated the influence of the interaction cutoff and water model on the surface-pressure area isotherms of DPPC monolayers, where the phospholipid and water molecules were modeled atomistically. Employing the Berger *et al.* [23] force field, with the TIP4P/2005 water model, along with a long cut-off (1.7 nm), led to the accurate prediction of pressure-area isotherms and reproduced the LE-LC transition, observed in the experiments at 310 K [24].

A brief look at the literature shows that in recent years, several studies have been devoted to investigate the lipid-protein interactions, using the MD simulations. Although such simulations provide a detailed view of lipid-protein interactions, they are limited by the availability of accurate parameters, describing such interactions, and also the limited time that can be simulated. The good point is that in both areas, the advancement is extremely fast [25].

Bachar and Becker performed the MD simulation of a bee venom peptide (melittin) in a DPPC bilayer, to investigate the membrane disorder. Their results showed an increased level of disorder and structural deformation for lower-layer phospholipids, in the immediate vicinity of the peptide [26].

In a 2004 review, Lee [27] has outlined various molecular and physical explanations for the effects of lipids on intrinsic membrane protein function, mainly to answer that how lipids affect the activities of integral membrane proteins. Believing that lipid-protein interactions are best understood at the molecular level, using MD simulations, Lee concluded that both lipid and protein molecules will distort to provide the best mutual interactions, while this can in turn affect the protein's function.

Deol *et al.* [8] have investigated the lipid-protein interactions of two integral membrane proteins: KcsA (an α-helix bundle protein) and OmpA (a β-barrel protein). They came to the conclusion that both these proteins form significant interactions between their aromatic belts and the lipid head groups. The importance of snorkeling interactions of basic side chains with the phosphate groups of lipids was also discussed.

Kandasamy and Larson have performed MD simulations on the interactions of DPPC monolayers with SP-B_{1-25}, the truncated version of pulmonary surfactant protein, SP-B. Their results showed that the formation of persistent hydrogen bonds between the donor atoms of the protein and

the acceptors of the lipid head group, determine the position, orientation, and secondary structure of the peptide, in the membrane environment [28].

Cheng *et al.* have investigated the interactions of POPC and POPA lipids and cholesterols (CHOL) with an open and closed channel α4β2 nicotinic acetylcholine receptors (nAChR). They found no CHOL in cavities within single subunits, whereas POPA could access some non-annular sites, due to its smaller head group, but POPC could not easily reach there, because of the steric exclusion. POPA was reported to act both as an acceptor and a donor of hydrogen bonding, while POPC has only emerged as a H-bond acceptor [29].

In a 2012 study, Wang *et al.* [30] reported the MD simulations of antimicrobial peptide CM15 with the two model lipid bilayers, pure POPC and mixed POPG:POPC (1:2), investigating the mutual protein-lipid interactions. The peptide interaction was found to be stronger with the anionic POPG:POPC than the zwitterionic POPC, due to the electrostatic attraction between CM15 and the negatively charged POPG.

Lockart and Klimov employed the isobaric-isothermal replica exchange MD to assess the impact of Aβ monomer on the equilibrium properties of DMPC bilayer. They observed that the peptide reduces the density of lipids in the binding "footprint" and indents the bilayer, thus creating a lipid density depression [31].

It is worth mentioning that cationic lipids have been less considered in the computational studies, compared to the neutral and anionic lipid bilayers [32,33]. Positively charged lipids are important and known to create complexes with DNA for gene therapy [34,35] and are also attractive since they can be easily designed, synthesized and characterized [36].

In this study, we have employed the MD simulation approach to explore the microscopic interactions of a 61-residue polypeptide (PDB entry code: 1vry) with the three different model lipid bilayers. The 1vry PDB file describes the three-dimensional structure of the second and third transmembrane domains (TM23) of the α-1 subunit of Human GlyR, linked by the important 23 loop, at the atomistic resolution [37].

Here, we aim to unravel the mutual interactions of pure DPPC (dipalmitoyl phosphatidylcholine), mixed DPPC-DMPC (dimyristoyl phosphatidylcholine) and mixed DPPC-DMTAP (dimyristoyl trimethylammonium propane) bilayers, with the embedded TM23 part of the α-1 subunit of GlyR (TM23-GlyR). In this respect, distinct atomistic MD simulations were conducted on the following systems, once without and once with the integral protein:

- Pure DPPC bilayer with 128 lipids (simulated by two force fields: GROMOS 53A6 & GROMOS 43A1),
- Mixed phospholipid bilayer (DPPC60%-DMPC40%) and
- Mixed lipid bilayer (DPPC60%-DMTAP 40%).

So, MD simulations were performed on the eight distinct systems, where each of the 'lipid only' and 'protein-containing' systems were simulated for 10 ns and 200 ns, respectively, using the Gromacs simulation package (5.4.1) [38]. The statistical analysis on the equilibrated trajectories was accomplished in the contexts of several structural properties, such as root mean square deviation (RMSD), radius of gyration (Rg), radial distribution function (RDF), deuterium order parameter (DOP), area per lipid (APL), bilayer thickness, density profiles, hydrogen bonding and secondary structure changes, using the Gromacs implemented analysis tools. These assessments shed light on the context of mutual lipid-protein interactions.

We could determine how the presence of DMPC or DMTAP molecules affect the structure of pure DPPC bilayer, how TM23 part of the α-1 subunit of the GlyR interacts with these bilayers, and what are the mutual effects of lipid and protein molecules on each other.

In fact, the MD simulation approach zooms in the detailed interactions between protein and lipid molecules, and reveals their reciprocal effects. This study is important due to providing the molecular scale information on the real protein (TM23-GlyR) interactions, with cationic, zwitterionic and even mixed lipid bilayers.

COMPUTATIONAL METHODS

MD Simulation System Setup

As it was mentioned in the previous section, we are going to simulate eight distinct systems in similar circumstances, using the Gromacs simulation package. In order to easily distinguish and classify the simulated systems and their respected analyses, we have numbered them as follows:

System 1: Pure DPPC bilayer (GROMOS 53A6) with 128 lipids,
System 2: Pure DPPC bilayer (GROMOS 43A1) with 128 lipids,
System 3: Mixed phospholipid bilayer (DPPC 60%-DMPC 40%),
System 4: Mixed lipid bilayer (DPPC 60%-DMTAP 40%),
System 5: Pure DPPC bilayer (with 128 lipids) + TM23-GlyR (GROMOS 53A6),
System 6: Pure DPPC bilayer (with 128 lipids) + TM23-GlyR (GROMOS 43A1),
System 7: Mixed phospholipid bilayer (DPPC 60% -DMPC 40%) + TM23-GlyR,
System 8: Mixed lipid bilayer (DPPC 60%-DMTAP 40%) + TM23-GlyR.

Phospholipids are the major components of cell membranes, able to form lipid bilayers, due to their amphiphilic characteristic. Each phospholipid molecule is made up of two hydrophobic fatty acid tails, and a hydrophilic head, consisting of a phosphate group, where these two parts are linked together by a glycerol molecule.

DPPC and DMPC are the zwitterionic (neutral) phosphatidylcholine lipids, with the two saturated C16 and C14 hydrocarbon tails, respectively. They are zwitterionic lipids, by virtue of having a negative charge on the phosphate group and a positive charge on the quaternary ammonium group. The charged choline group acts as the surfactant head group interfacing with water and the acyl fatty acid chains to form the hydrophobic bulk of the lipid layers [39]. On the other hand, DMTAP is a cationic amphiphile lipid with two saturated C14 hydrocarbon tails (see Fig. S1).

In order to construct the starting configurations for the lipid membrane systems, the Membuilder web server [40] was employed. The accuracy of MD simulations of membranes mainly depends on the quality of membrane models and the applied force fields. Membuilder is a web-based graphical interface, able to build heterogeneously mixed membrane bilayers for the GROMACS simulation program. Using this server, the type and quantity of our intended lipids were specified for each membrane layer, where simple point charge (SPC) water molecules solvated the bilayer on both sides.

The Membuilder web-server has listed the lipids and their corresponding force fields. For DPPC, both GROMOS 53A6 and GROMOS 43A1 force fields were available, but for DMPC and DMTAP, only GROMOS 53A6 and GROMOS 43A1 were accessible, respectively. In order to simulate the mixed bilayer systems, it is better for the both lipid systems to have the same force field, so, we simulated the pure DPPC bilayer with both force fields, to become able to mix it later with DMPC or DMTAP lipids. Table 1 summarizes the characteristics of our studied model membranes.

On the other hand, the 3D structure of TM23-GlyR with the pdb code of 1vry was taken from the orientations of proteins in membrane (OPM) database [41]. OPM provides the spatial arrangements of membrane proteins with respect to the hydrocarbon core of the lipid bilayer.

In order to create the initial configurations for the systems (5-8), the computational tool, called g_membed (Part of the Gromacs suite of programs), was employed to insert TM23-GlyR into each of the systems (1-4). The g_membed tool embeds a membrane protein into an equilibrated lipid bilayer, at the user specified position and orientation. So, the required inputs for this program are the equilibrated membrane system, and the protein structure in the right position and orientation with respect to the lipid bilayer [42].

g_membed first decreases the width of the protein in the xy-plane and removes all the lipid and water molecules, overlapping with the narrowed protein. Then, the protein is grown back to its full size in a short molecular dynamics simulation (around 1000 steps), while pushing the lipids away to accommodate the membrane protein in a favorable way. In this study, after an insertion of TM23-GlyR in the four lipid membranes, only a short equilibration run (1 ns) was required to re-equilibrate the membranes.

The net +3 charge on the TM23-GlyR was neutralized by adding 3 Cl^- (Chloride) ions, as neutralizing counter-ions. In the case of DMTAP containing systems, necessary number of anions were also added to neutralize the cationic lipid molecules. Under Gromacs, the most widely-used parameters for the lipid simulations are called “Berger Lipids”, derived by Berger *et al*. [23].

The Berger force field is a united atom lipid force field, where bonds, angles and dihedrals have been taken from GROMOS87. Since the long alkane chains are poorly

Table 1. Studied Model Membranes

Membrane	Force field	Number of lipids	Percent of lipids
Pure DPPC bilayer (Systems 1 & 2)	1) GROMOS 53A6	DPPC: 128	DPPC: 100%
	-	-	-
	2) GROMOS 43A1	DPPC: 128	DPPC: 100%
Mixed phospholipid bilayer (DPPC 60%-DMPC 40%) (System 3)	GROMOS 53A6	DPPC: 76 DMPC: 52	DPPC: 60% DMPC: 40%
Mixed lipid bilayer (DPPC 60%-DMTAP 40%) (System 4)	GROMOS 43A1	DPPC: 76 DMTAP: 52	DPPC: 60% DMTAP: 40%

represented by GROMOS bonded parameters, a Ryckaert-Bellemans dihedral potential has been used for the lipid tails [43,44]. The LJ parameters were taken from OPLS and charges from the Chiu *et al*. paper [45].

In order to perform the MD simulations of systems (5-8), containing both lipid and protein molecules, the Berger lipid parameters needed to be combined with a GROMOS representation of the TM23-GlyR protein. In this respect, the protocol described by Justin Lemkul was employed to combine the lipid and protein topologies [46].

Molecular Dynamics Simulation Details

Before the real MD simulations or at the beginning of dynamics, it should be ensured that the systems has no steric clashes or inappropriate geometry. So, all studied systems were first energy minimized for 50000 steps, using the steepest descent algorithm, [47] to relax the structures and release the conflicting contacts.

The equilibration process was conducted through a short NVT phase, followed by a longer NPT one. The equilibration under the NVT ensemble was carried out for 100 ps, while the protein was position restrained by force constant of 1000 kJ mol^{-1} nm^{-2}. During the heating process, temperature was increased from 0 to 323 K by rescaling the velocities, until the target temperature was achieved. This temperature was defined above the gel-to-liquid phase transition temperature of the lipid bilayers, using the Nose-Hoover thermostat. The NPT equilibration phase was then conducted for 1000 ps (1 ns), where the pressure was maintained at 1 bar, using the Parrinello-Rahman barostat [48].

In a membrane protein simulation, the need for longer NPT phase is due to the heterogeneity of the system, where both water and DPPC molecules act as solvents for the membrane protein. Such heterogeneity requires a longer equilibration process to let the water molecules re-orient around the lipid head-groups and any exposed parts of the protein. On the other hand, the lipids must orient themselves around the membrane protein (TM23-GlyR) as well [46].

Upon completion of these two equilibration phases, the eight simulated systems became well-equilibrated at the desired temperature and pressure. So, in the next step, the position restraints were released and the lipid systems and protein-containing systems were respectively subjected to 10 ns and 200 ns production MD for data collection. All MD simulations and minimizations were carried out with the Gromacs 5.4.1 package [39], using the previously mentioned force fields.

It should be noted that the periodic boundary conditions (PBC) were applied in the 3 box dimensions to reduce the boundary effects. The Newtonian equations of motion were integrated using the leap-frog algorithm with a time step of 2 fs. The non-bonded van der Waals and electrostatic interactions were truncated smoothly at 1.4 nm for all the atom pairs. The efficient Particle Mesh Ewald (PME) [49] method was used to represent the long-range electrostatics, where the grid spacing for fast Fourier transform (FFT) was set to 0.16. Finally, VMD [50] and pymol [51] softwares were utilized to visualize the MD simulation boxes.

RESULTS AND DISCUSSION

By simulating the eight systems, introduced in the methods section, first we were going to analyze the effect of adding DMPC or DMTAP molecules on the structure of pure DPPC bilayer, while in the next step, TM23-GlyR was added to the lipid bilayers to assess the mutual interactions of lipid and protein molecules.

In this respect, each system of 1-4 (containing only lipid molecules) was simulated for 10 ns at 323 K and their state of equilibrium was examined through analyzing the roost mean square deviation and the simulation box-x length. After addition of TM23-GlyR to the equilibrated lipid bilayers, each protein containing system was simulated for 200 ns and further structural analyzes were performed to elucidate different aspects of lipid-protein interactions.

Root Mean Square Deviation (RMSD)

At the end of 10 ns simulation of systems 1-4, the time evolution of root mean square deviation (RMSD) plots of DPPC molecules were analyzed in order to examine the convergence of MD simulations towards equilibrium. Figure S2 shows the RMSD values of DPPC molecules, as a function of simulation time. It can be seen that for the 4 lipid systems, first RMSD increases by almost two units, then it oscillates around an average value after 7 ns, persuading us that the studied systems are in equilibrium status after 10 ns. These systems were later used as lipid bilayer hosts for the TM23-GlyR membrane protein.

Comparing the RMSD plots for systems 3: (DPPC60%-DMPC40%) and 4: (DPPC60%-DMTAP40%) reveals that adding DMTAP molecules to the pure DPPC bilayer has more effect on the structural properties of DPPC molecules. It is expected that all other structural properties of system 4 show more obvious changes compared to the corresponding properties of system 3.

MD Simulation Box Length

Figure S3 shows the time evolution of Box-x length of simulation boxes for systems 1-4, obviously indicating that after about 7 ns, box-x lengths oscillate around a constant value. A close inspection of plots in Fig. S3 shows that inserting 40% DMPC molecules leads to an increase in the box-x length, while adding DMTAP molecules decreases the box dimension.

The DPPC and DMPC molecules have different hydrocarbon chain lengths, so DPPC molecules shorten their alkyl lengths to maximize the non-polar interactions with the shorter chains of DMPC molecules. This is the reason behind the increase in the box-x length of system 3, in comparison to the system 1. It is worth mentioning that when lipid molecules stand straight and packed, their area per lipid would decrease, leading to the shorter box length. The clear decrease in the box length of system 4: (DPPC60%-DMTAP40%) compared to the system 2: (pure DPPC, GROMOS 43A1) may be attributed to the cationic nature of DMTAP head groups enabling them to establish electrostatic interactions with the zwitterionic head groups of DPPC molecules. These strong interactions lead to the smaller area per lipid for DPPC and DMTAP molecules, resulting in shorter box-x length.

It should be mentioned that the box-x lengths of starting structure files of all 1-4 lipid systems (taken from Membuilder) were 6.4 nm, while the initial box-x values, shown in Fig. S3, differ obviously from systems (1 and 3) to the systems (2 and 4). The reason is that the graphs in Fig. S3 show only the box-x evolution of the MD step of the simulation process, while the systems have passed energy minimization and two equilibration phases (NVT & NPT) prior to that.

When the equilibrium status of the lipid systems was confirmed through the RMSD and box length analyses, TM23-GlyR was inserted to the bilayer systems (1-4) to create the initial structures of systems (5-8). All systems containing protein were subjected to MD simulations for 200 ns. As mentioned in the computational methods section,

these protein containing bilayers are at their minimum energy states and simulated under position restrained conditions before the real MD step of 200 ns. In the following trajectory analysis, we have mainly focused on the two sets of systems: (1, 3 and 7) and (2, 4 and 8). This arrangement enables us to monitor first the effect of inserting DMPC (or DMTAP) molecules on the pure DPPC bilayer, and then the impact of adding TM23-GlyR to the mixed bilayer system.

Radial Distribution Function (RDF)

Pair correlation functions or the radial distribution functions (RDF) of the three middle carbon atoms of DPPC chains (*sn*-1 and *sn*-2), were used to examine the state of order of these lipid molecules. The liquid condensed phase is characterized by the existence of long-range order in the lipid RDF plots [52].

Figure 1 demonstrates the RDF plots for *sn*-1 chains of DPPC molecules in systems 1, 3 and 7. By adding 40% of DMPC molecules to the pure DPPC bilayer, the height of first peak in the RDF plot was decreased from 1.4 to 1.2, which is mainly due to decrease the number of DPPC molecules compared to the system 1 containing 100% DPPC molecules. Looking at other RDF peaks of systems 1 and 3 shows no detectable change in the long range behavior and subsequently the state of order of DPPC molecules, after substituting 52 DPPC molecules (out of 128) with the DMPC ones. The vertical axis in the RDF plot is the measure of probability of finding a particle at a distance *r*, away from a given reference particle relative to that for an ideal gas. So, replacing 52 DPPC molecules with the DMPC lipids leads to the height decrease of RDF peaks, directly due to the decrease in the number of DPPC molecules around the reference lipid.

Later, when TM23-GlyR was added to the mixed bilayer system, although few DPPC and DMPC molecules were deleted by the g_membed tool (to find enough space for the membrane protein), distinguishable increase in the height of first RDF peak of DPPC molecules was observed. This indicates the role of this membrane protein in increasing the order state of DPPC molecules. This effect was also observed in the deuterium order parameter plots discussed later.

On the other hand, inspecting Fig. 2 shows that adding 40% DMTAP molecules to the pure DPPC bilayer also leads to the decrease in the height of first RDF peak, which again is due to the population decrease of DPPC molecules. Considering Figs. 1 and 2 simultaneously, and comparing the RDF plots of systems 7 (DPPC60%-DMPC40% + TM23-GlyR) and 8 (DPPC60%-DMTAP40% + TM23-GlyR) demonstrates a considerable increase in the long range order of DPPC molecules in system 8. Both systems 7 and 8 have the same number of DPPC molecules, while presence of cationic DMTAP molecules in system 8 led to the stronger interactions with DPPC lipids and also TM23-GlyR, which in turn, leads to the decrease in the area per lipid of both DPPC and DMTAP molecules, and so higher order arrangement of DPPC lipids.

Deuterium Order Parameter (S_{CD})

One of the most common properties, analyzed in the molecular dynamics simulations of phospholipids, is the order parameter of lipid acyl chain tails. These order parameters provide information regarding both the overall order of the membrane and specific details of the conformations that the atoms within the lipid tails adopt [53]. The lipid tail deuterium order parameter, S_{CD}, is a measure of the orientation and ordering of the phospholipid tails in the bilayer with respect to the bilayer normal [54]. More and less ordered structures give rise to the high and low values of order parameters, respectively.

Figures 3 and 4 show the deuterium order parameters, S_{CD}, for the *sn*-1 and *sn*-2 chains of DPPC molecules, for systems (1, 3 and 7) and (2, 4 and 8), respectively. It should be mentioned that the order parameters are normally defined for all saturated carbons containing two neighboring carbon atoms, so for DPPC, these parameters can be calculated only for atoms C_2 to C_{15}. On the other hand, usually, the order parameters for the two hydrocarbon chains (*sn*-1 & *sn*-2) are analyzed separately, even for DPPC with two acyl chains, each having 16 carbon atoms, because the distance between the two hydrocarbon tails and the water-bilayer interface are not equivalent [55].

Figure 3 shows the lower deuterium order parameter values for both *sn*-1 and *sn*-2 chains of DPPC molecules in system 3 (DPPC60%-DMPC40%) compared to the system 1 (pure DPPC, GROMOS 53A6). This is clearly an indication of order loss after adding 40% DMPC molecules to the pure

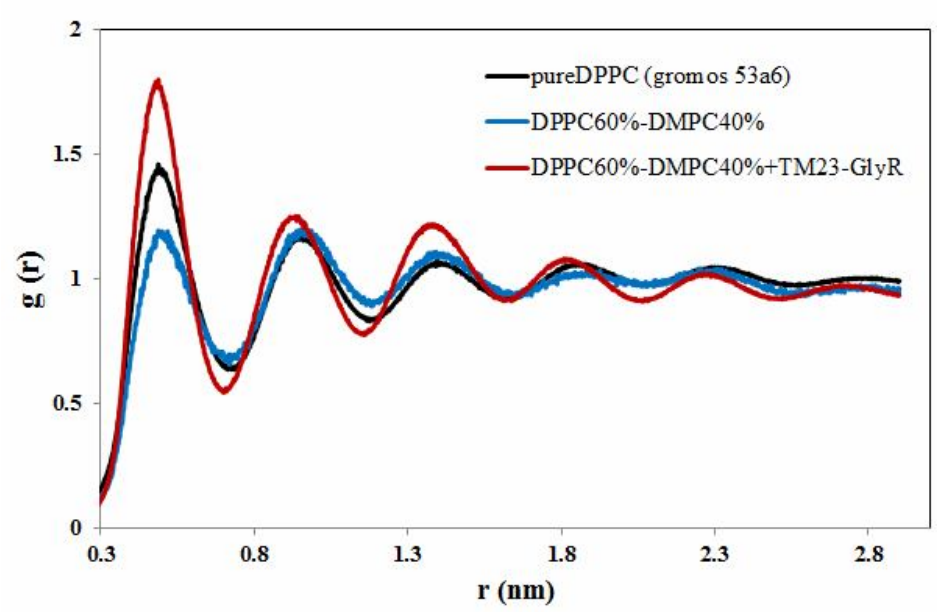

Fig. 1. Radial distribution functions (RDF) of three middle carbon atoms in the *sn*-1 chains of DPPC molecules, for systems 1, pure DPPC (GROMOS 53A6), 3, (DPPC60%-DMPC40%) and 7, (DPPC60%-DMPC40% + TM23-GlyR).

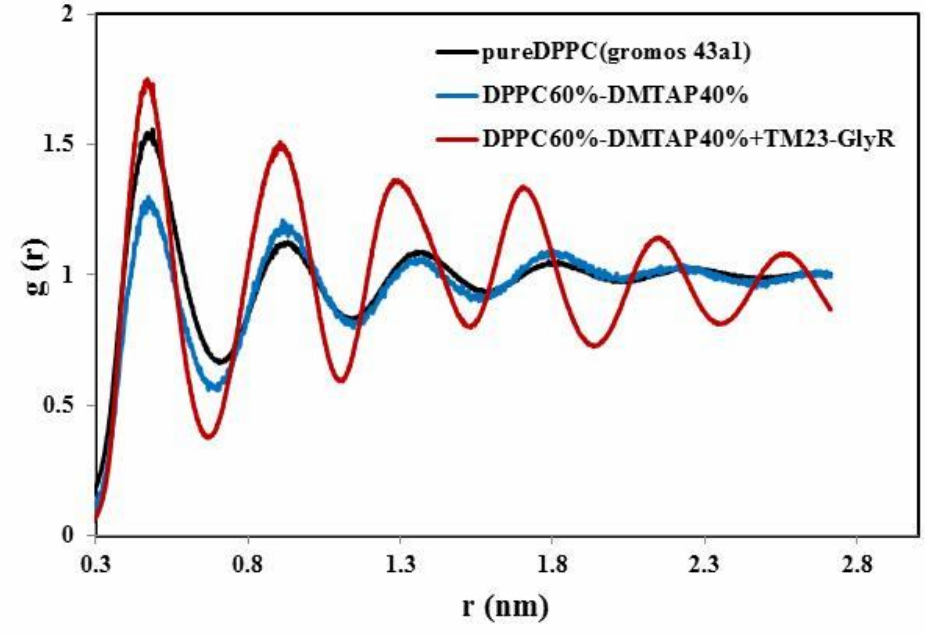

Fig. 2. Radial distribution functions (RDF) of three middle carbon atoms in the *sn*-1 chains of DPPC molecules for systems, 2, pure DPPC (GROMOS 43A1), 4, (DPPC60%-DMTAP40%) and 8, (DPPC60%-DMTAP40% + TM23-GlyR).

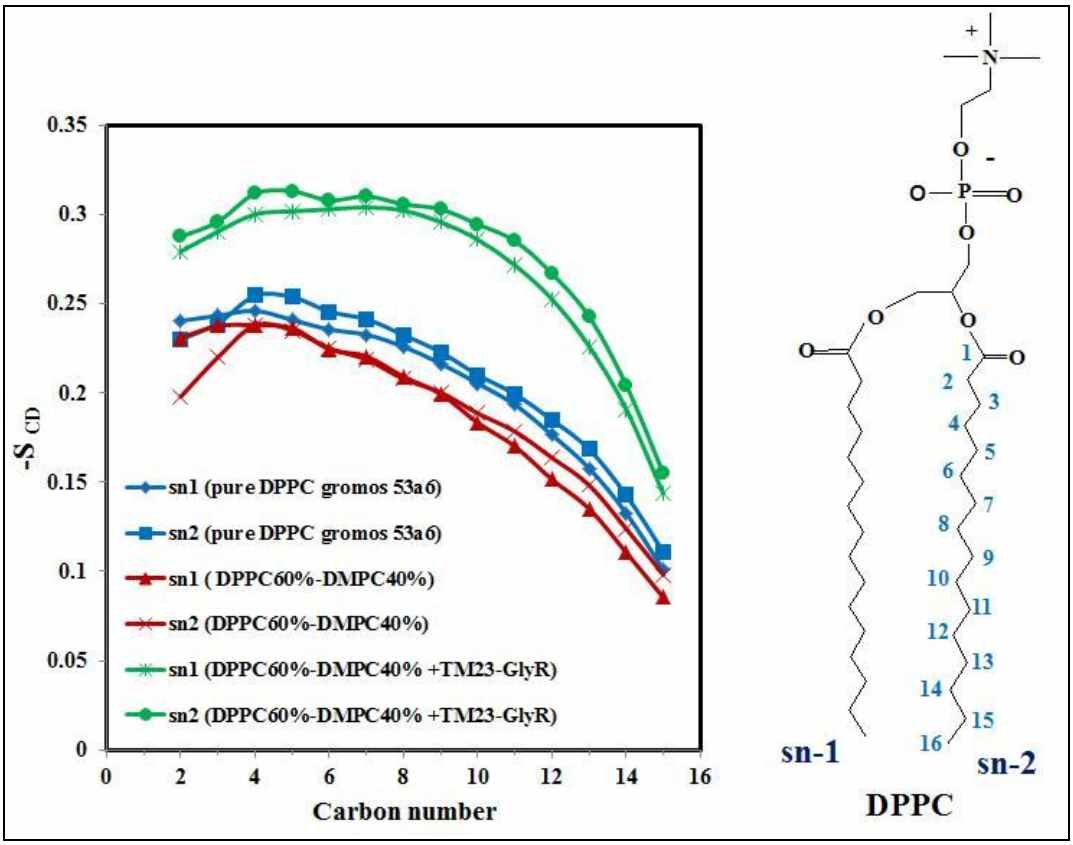

Fig. 3. Deuterium order parameter, S_{CD}, for *sn*-1 and *sn*-2 chains of DPPC molecules of systems: 1, pure DPPC (GROMOS 53A6), 3, (DPPC60%-DMPC40%) and 7, (DPPC60%-DMPC40% + TM23-GlyR).

Table 2. The Area per Lipid of DPPC Head Groups for the Top and Bottom Leaflets of the Bilayer Systems: 1, Pure DPPC (GROMOS 53A6), 3, (DPPC60%-DMPC40%) and 7, (DPPC60%-DMPC40% + TM23-GlyR)

System	Area per lipid (nm^2)
Pure DPPC (GROMOS 53A6)	Top: 0.605 ± 0.004
(system 1)	Bottom: 0.605 ± 0.004
DPPC60%-DMPC40%	Top: 0.611 ± 0.005
(system 3)	Bottom: 0.611 ± 0.005
DPPC60%-DMPC40% + TM23-GlyR	Top: 0.484 ± 0.007
(system 7)	Bottom: 0.541 ± 0.012

DPPC bilayer. As mentioned before, the difference in the hydrocarbon chain lengths of DPPC and DMPC molecules forces the DPPC lipids to shorten their hydrophobic tails, in order to establish more effective non-polar interactions with hydrocarbon tails of DMPC molecules.

Higher S_{CD} values for both *sn*-1 and *sn*-2 chains of DPPC molecules in system 7 (DPPC60%-DMPC40% + TM23-GlyR) indicates the clear increase of DPPC chain order after adding TM23-GlyR to the system. The same increase in the deuterium order parameters of DPPC chains, in response to the presence of membrane protein, has also been reported in previous studies [56].

Figure 4 represents higher deuterium order parameters for DPPC hydrocarbon tails of system 4 (DPPC60%-DMTAP40%) compared to the system 2 (pure DPPC, GROMOS 43A1). It is clear that replacing 40% of DPPC molecules with the DMTAP lipids leads to the more ordered DPPC chains. Later addition of TM23-GlyR and creation of system 8 (DPPC60%-DMTAP40% + TM23-GlyR) also gives rise to the further distinguished increase in the S_{CD} values for both *sn*-1 and *sn*-2 DPPC chains. Comparing Figs. 3 and 4 shows that the maximum value of S_{CD} is around 0.3 for system 7, while it is about 0.38 for DPPC chains of system 8. This is due to the different nature of intermolecular interactions in these systems, where the electrostatic interactions are responsible for higher chain order in system 8, due to having cationic DMTAP lipids. These observations are in accordance with the results for box-x lengths and radial distribution functions of these systems.

Area per Lipid and Bilayer Thickness

Area per lipid (APL) and bilayer thickness are other two properties commonly analyzed in lipid MD simulations. The GridMAT-MD tool [57] is a simple perl script designed to calculate these two parameters. This program is particularly useful in the case of embedded membrane proteins, because it can calculate the APL, while still compensating for the lateral area occupied by the protein at the intersection with the membrane interface. The area per lipid is calculated as the lateral area of the simulation box, divided by the number of lipids in each leaflet.

Table 2 shows the APL values of the top and bottom leaflets of the pure and mixed bilayer systems, 1, 3 and 7. Comparing the APL values for systems 1 and 3 shows that replacing 40% of DPPC lipids with the DMPC molecules increases the average APL of DPPC lipids from 0.605 to 0.611 nm^2. Although this is a small change, it is large enough to lead to the decrease of deuterium order parameters of DPPC acyl chains for system 3 with respect to system 1, as discussed before. It is worth mentioning that these values also are in accordance with the increased box-x length for system 3; discussed in the 1.3.2 section.

Later addition of TM23-GlyR, leading to system 7, gives rise to the subtle decrease in the APL of DPPC lipids to become 0.484 and 0.541 nm^2 for the top and bottom leaflets, respectively. Again, this considerable reduction of APL value is consistent with the results of deuterium order parameters, radial distribution functions and even box-x lengths. Asymmetric change in the APL values of top and bottom leaflets may be attributed to the different interactions of the TM23-GlyR residues with these two leaflets.

As shown in Table 3, the APL values of system 4 show 0.03 nm^2 decrease compared to the ones for system 2, in both top and bottom leaflets. This observation which is compatible to the box-x and S_{CD} analyzes confirms again that substitution of 40% of DPPC molecules, with DMTAP lipids, leads to the more order in the arrangement of DPPC chains.

Subsequent insertion of TM23-GlyR protein leads to the 0.116 and 0.141 nm^2 decrease in APL values of the top and bottom leaflets of system 8 in comparison to the system 4. Again, an uneven change in the APL values of the two leaflets is observed. The smaller head groups of DMTAP cationic lipids compared to DPPC head groups, the strong electrostatic interactions between the head groups of DMTAP and DPPC lipids, and also interactions of both lipids with the membrane protein, TM23-GlyR, are responsible for the considerable decrease in the APL values of DPPC molecules in system 8.

In Table 4, the APL head groups of the DPPC lipids are analyzed and compared from another point of view. Here, only the four protein containing systems are considered, namely the systems 5, 6, 7 and 8. The second and third columns of Table 4 list the APL values of both the top and bottom leaflets of the mentioned systems, at t = 0 and t = 200 ns, respectively. This way, we are going to assess

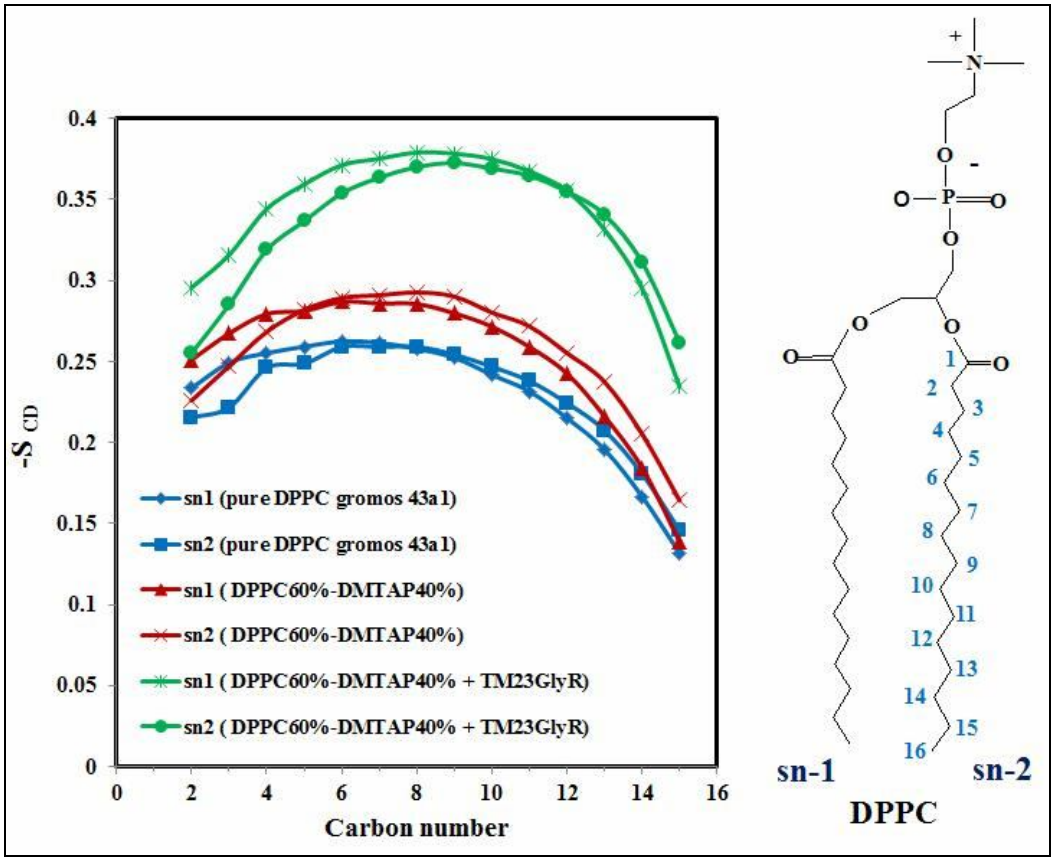

Fig. 4. Deuterium order parameter, S_{CD}, for *sn*-1 and *sn*-2 chains of DPPC molecules of systems: 2, pure DPPC (GROMOS 43A1), 4, (DPPC60%-DMTAP40%) and 8, (DPPC60%-DMTAP40%+TM23-GlyR).

Table 3. The Area per Lipid of DPPC Head Groups for the Top and Bottom Leaflets of the Bilayer Systems: 2, Pure DPPC (GROMOS 43A1), 4, (DPPC60%-DMTAP40%) and 8, (DPPC60%-DMTAP40% + TM23-GlyR

System	Area per lipid (nm^2)
Pure DPPC (GROMOS 43A1)	Top: 0.549 ± 0.009
(system 2)	Bottom: 0.549 ± 0.009
DPPC60%-DMTAP40%	Top: 0.519 ± 0.007
(system 4)	Bottom: 0.519 ± 0.007
DPPC60%-DMTAP40% + TM23-GlyR	Top: 0.403 ± 0.014
(system 8)	Bottom: 0.378 ± 0.014

Table 4. The Area per Lipid of DPPC Head Groups for the Top and Bottom Leaflets of the Four Protein-containing Systems: System 5, [Pure DPPC (GROMOS 53A6) + TM23-GlyR], System 6, [Pure DPPC (GROMOS 43A1) + TM23-GlyR], System 7, (DPPC60%-DMPC40% + TM23-GlyR), and System 8 (DPPC60%-DMTAP40% + TM23-GlyR)

System	Area per lipid (nm^2) t = 0 ns	Area per lipid (nm^2) t = 200 ns
Pure DPPC (GROMOS 53A6)+ TM23-GlyR (system 5)	Top: 0.557 ± 0.007 Bottom: 0.566 ± 0.009	Top: 0.476 ± 0.006 Bottom: 0.522 ± .007
Pure DPPC (GROMOS 43A1) + TM23-GlyR (System 6)	Top: 0.540 ± 0.010 Bottom: 0.541 ± 0.015	Top: 0.499 ± 0.009 Bottom: 0.497 ± 0.010
DPPC60%-DMPC40% + TM23-GlyR (system 7)	Top: 0.570 ± 0.006 Bottom: 0.574 ± 0.008	Top: 0.484 ± 0.007 Bottom: 0.541 ± 0.012
DPPC60%-DMTAP40% + TM23-GlyR (system 8)	Top: 0.464 ± 0.011 Bottom: 0.439 ± 0.016	Top: 0.403 ± 0.014 Bottom: 0.378 ± 0.014

Table 5. Average Bilayer Thicknesses of the Systems: 1, Pure DPPC (GROMOS 53A6), 3, (DPPC60%-DMPC40%) and 7, (DPPC60%-DMPC40%+TM23-GlyR)

System	Average Bilayer thickness (nm)
Pure DPPC (GROMOS 53A6) (system 1)	3.940 ± 0.022
DPPC60%-DMPC40% (system 3)	3.718 ± 0.055
DPPC60%-DMPC40% + TM23-GlyR (system 7)	4.298 ± 0.031

how this parameter changes in the course of the simulation runs.

It is clear that for all mentioned protein containing systems, APL decreases with time. This is mainly due to the established interactions of TM23-GlyR protein with the lipids, holding them more packed together, decreasing the dimensions of simulation box, and subsequently the average cross-sectional area per lipid. The systems 5 and 6 are both consisted of pure DPPC bilayer + TM23-GlyR protein, while the only difference between them is the employed force field for the simulation of DPPC molecules.

As shown in Fig. 3, the Box-x dimension of system 1 (Pure DPPC bilayer, GROMOS 53A6) is larger than system 2 (Pure DPPC bilayer, GROMOS 43A1), and as reported in Tables 2 and 3, the APL values for these systems are respectively 0.605 and 0.549 nm. Systems 1 and 2, after an addition of the membrane protein, have been named 5 and 6, respectively. Different APL values of DPPC molecules in systems 5 and 6, specially at the end of 200 ns simulation, may be attributed to the differences of GROMOS 53a6 and GROMOS 43a1 force fields, because both systems contain 100% DPPC molecules, along with the same inserted membrane protein. It is worth mentioning that D. Poger and A. E. Mark [58] have claimed that the area per lipid, which is often used to assess the validity of the force fields and the convergence of the simulations, is relatively insensitive to the force field nature and the method used to treat the long range electrostatics. However, in this study the effect of force field on the APL value was found not to be negligible.

In the case of systems 7 (DPPC60%-DMPC40% + TM23-GlyR) and 8 (DPPC60%-DMTAP40% + TM23-GlyR), greater difference is observed between the APL values, both at the start and end of the simulation times. Again part of this difference may be attributed to the disparities of the employed force fields in simulation of the lipid systems, while the main part is because of the stronger interactions of DMTAP lipid molecules with the membrane protein compared to the DMPC phospholipids. In the discussion of Figs. 3 and 4, it was explained how the nature of lipid-protein interactions affects the order of lipid systems. System 8 shows lower APL values for the DPPC molecules (compared to system 7), which is in reasonable accordance with the higher deuterium order parameter values of sn-1 and sn-2 chains of its DPPC lipids.

The hydrophobic match between a membrane protein and its host lipid bilayer is one of the core features in the context of the lipid bilayer-integral membrane protein interactions. Minimizing the energetic penalty associated with exposing a nonpolar/polar interface is the driving force for the membrane protein and its neighbor lipid molecules to mutually adjust the lengths of their hydrophobic sections [59].

In this study, the lipid bilayer thickness, namely, the head group-head group separation, was calculated using the GridMAT-MD tool. This program measures the bilayer thickness in terms of P-P distance between the top and bottom leaflets generating the data for a top-down perspective of the lipid bilayer [57,60].

Tables 5 and 6 report the average bilayer thicknesses of systems (1, 3 and 7) and (2, 4 and 8), respectively. In fact, the output structure file of each simulation run was employed to calculate the bilayer thickness, using the GridMAT-MD tool. The lower bilayer thickness of system 3 compared to system 1, and higher value of this property for system 7 are both in accordance with other analyzed properties, namely, deuterium order parameters and area per lipids. According to Kucerka *et al.*, at any given temperature, the area per lipid decreases, while the bilayer thickness increases with increasing the acyl length [61]. This observation has been attributed to the stronger van der Waals attraction for longer lipid chains.

In this respect, when 40% of DPPC molecules are substituted by DMPCs with the shorter acyl lengths, the result of lower bilayer thickness (for system 3) is completely conceivable. On the other hand, higher bilayer thickness of system 7 compared to system 3, with the same lipid composition, is due to the presence of TM23-GlyR membrane protein, which establishes further interactions with both lipid molecules, leading to the lower area per lipid and subsequently higher bilayer thickness.

When it comes to the systems (2, 4 and 8), the reported data in Table 6 reveal that substituting 40% of DPPC lipids with DMTAP leads to the slight decrease in the bilayer thickness. Although analysis of deuterium order parameters of DPPC molecules, in Fig. 4, showed that adding 40% of DMTAP lipids results in increasing the order of DPPC molecules, the corresponding bilayer thickness does not

Table 6. Average Bilayer Thicknesses of the Systems: 2, Pure DPPC (GROMOS 43A1), 4, (DPPC60%-DMTAP40%) and 8, (DPPC60%-DMTAP40% + TM23-GlyR)

System	Average Bilayer thickness (nm)
Pure DPPC (GROMOS 43A1) (system 2)	4.025 ± 0.074
DPPC60%-DMTAP40% (system 4)	3.957 ± 0.058
DPPC60%-DMTAP40% + TM23-GlyR (system 8)	4.465 ± 0.044

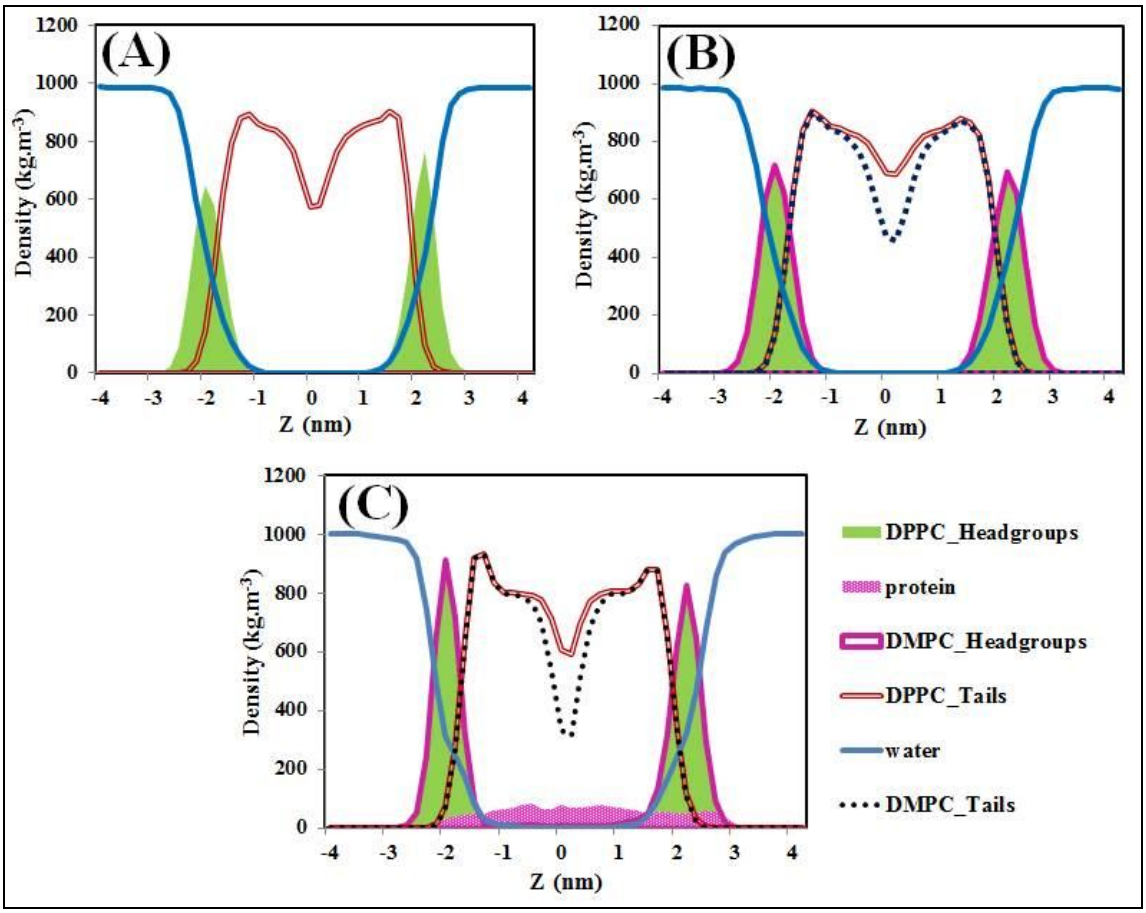

Fig. 5. Density profiles of membrane components, along the membrane normal direction, obtained from the trajectories of A) System 1, Pure DPPC (GROMOS 53A6), B) System 3, (DPPC60%-DMPC40%), and C) System 7, (DPPC60%-DMPC40% + TM23-GlyR).

show the expected increase. This may be attributed to the fact that bilayer thickness is the calculated P-P distance between the two leaflets of the membrane, while deuterium order parameter depends on the order and length of hydrocarbon chains. Due to the lower area per lipid in system 4, the head groups of DPPC molecules are oriented in a way that the P-P distance shows a little decrease from system 2 to the system 4. On the other hand, addition of TM23-GlyR to the mixed DPPC 60%-DMTAP 40% bilayer induces a considerable increase in the bilayer thickness, which is in exact agreement with the analyzed area per lipids and deuterium order parameters for system 8.

On the other hand, calculated bilayer thicknesses using the GridMAT-MD can be represented as two dimensional contour plots colored according to the bilayer thickness which provide a convenient way to depict this property. Figure S4 illustrates the membrane thickness contour plots of the first (t = 0 ns) and last (t = 200 ns) MD configurations, in the systems containing protein (5, 6, 7 and 8). As seen in Fig. S4, both the horizontal and vertical axes have the same grid number (the number of grid points across each axis, x & y). Here, the gird number of 200 has generated a grid that is 200 × 200 points or 40,000 points in total. A smaller grid number (20 to 25) will generate data that looks like a smooth gradient useful for observing changes in the thickness of the lipid bilayer. A larger grid order (100 to 200) generates data that looks more like a tessellation that is useful for determining individual areas per lipid head group. It is obvious that regions of increased membrane thickness contain higher ordered lipid molecules. On the other hand, integral membrane proteins are known to significantly alter the structure of their surrounding lipid environment [62].

Inspecting Fig. S4 shows that in all systems (5, 6, 7 and 8), the overall membrane thickness has been increased significantly at the end of simulation time, especially in the middle of the simulation box, where the membrane protein exists. According to the deuterium order parameter analysis, system 8 showed high SCD values for both sn-1 and sn-2 DPPC chains, where correspondingly, its membrane thickness contour plot (Figs. S4-D) displays the most homogenous distribution of highly ordered regions, when compared to the systems 5, 6 and 7. This observation confirms once again the effective role of mutual interactions of TM23-GlyR, DPPC and DMTAP molecules, in increasing the bilayer thickness and deuterium order parameters, along with the decrease in the area per lipid molecules.

Mass Density Profiles

Another commonly calculated parameter in molecular dynamics simulations of bilayer membranes is the mass density profile across the bilayer, demonstrating how mass is distributed along the membrane z-axis. The initial step in calculating this parameter is to determine the center of mass (COM) coordinates of the membrane, namely the COM of the two membrane leaflets. Later, in order to generate the mass density profile, the position coordinates (x, y, z) of all atoms are determined relative to the instantaneous COM (z = 0). It is called instantaneous because it can fluctuate during the simulation course [63]. Figures 5 and 6 depict mass density profiles of membrane components along the normal direction (z-axis), obtained from the equilibrated trajectories (Fig. 5: systems 1, 3 and 7, Fig. 6: systems 2, 4 and 8).

Density profile of DPPC molecules in Fig. 5A demonstrates the characteristic common picture of a bilayer structure, where the lipid molecules aggregate to bury their hydrophobic tails in the interior and expose their hydrophilic heads to the water layer. Due to the equal number of lipids in both leaflets, the density profile along the z-direction is almost symmetric around the bilayer center, located at z = 0 nm. Mass density for DPPC tails peaks at about 0.9 g cm^{-3}, while in the middle of bilayer membrane, density is meaningfully lower, reduced to 0.6 g cm^{-3}, showing a well near the DPPC bilayer center.

In Fig. 5B, showing the density profiles of system 3, DPPC tails interdigitate more strongly than DMPC tails across the membrane center. This is due to the fact that hydrocarbon chains of DPPC lipids are two carbon longer than those of DMPC ones. When it comes to the density profiles of DPPC and DMPC head groups, complete conformity is observed, because they have the same hydrophilic head groups.

Figure 5C depicts density profiles of membrane components of system 7. Comparing this figure with Fig. 5B reveals that the head group densities of both DPPC and DMPC lipids show an evident increase to higher than

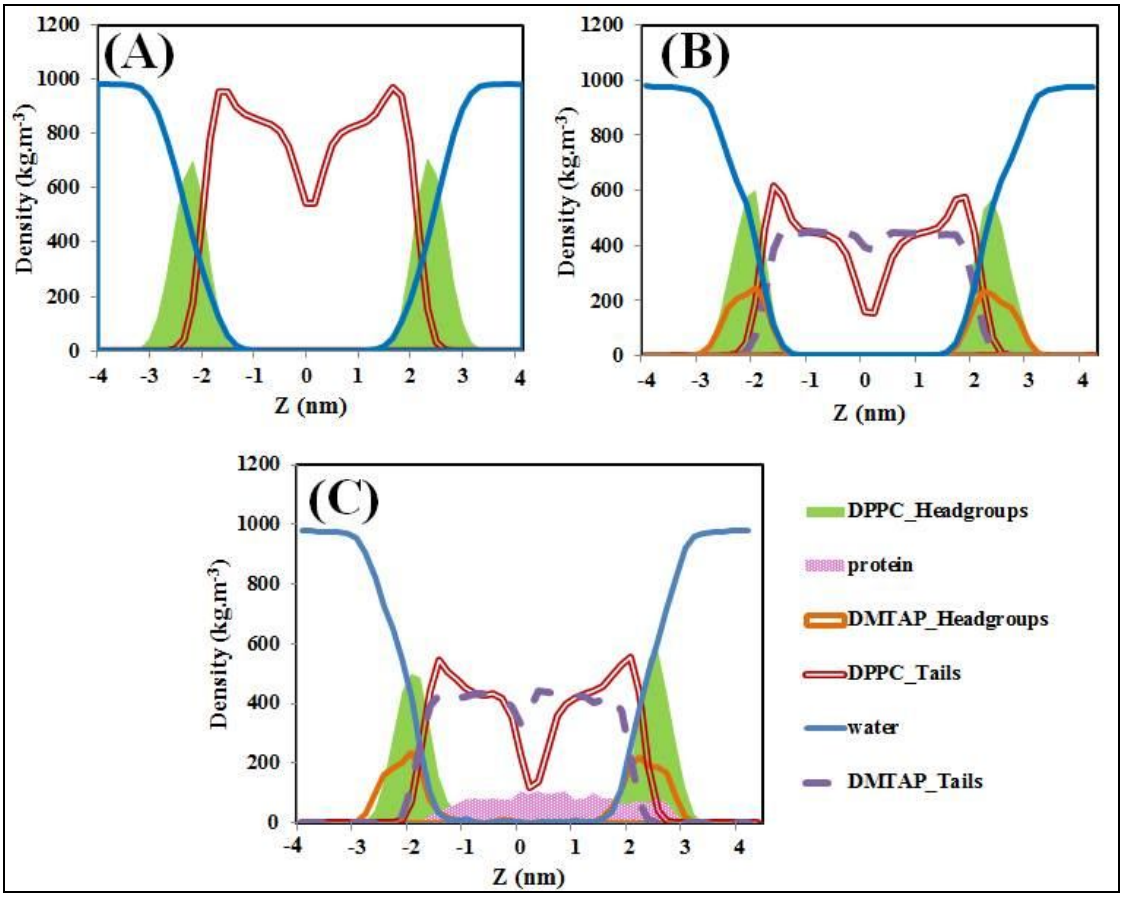

Fig. 6. Density profiles of membrane components, along the membrane normal direction, obtained from the trajectories of A) System 2, pure DPPC (GROMOS 43A1), B) System 4, DPPC60%-DMTAP40%, and C) System 8, DPPC60%-DMTAP40%+TM23-GlyR.

0.8 g cm^{-3}, in accordance with the lower area per lipid head group of system 7 compared to system 3. On the other hand, mass densities of DPPC and DMPC tails show an observable decrease in the bilayer center, which is compatible with the higher bilayer thickness in the presence of TM23-GlyR.

Figure 6A shows the density profiles of membrane components of system 2, which is similar to Fig. 6A for system 1, with the only difference that here DPPC lipids have been simulated using the GROMOS 43A1 force field. When 40% of DPPC molecules are replaced by DMTAP lipids, Fig. 6B shows dramatic decrease in the densities of DPPC tails, partly due to the reduction in the number of DPPC molecules and partly due to the increase of order in DPPC chains, in the presence of DMTAP lipids. The lower head group densities of DMTAP molecules compared to the DMPC ones are related to their smaller head parts. Considering the density profiles of system 8, where the TM23-GlyR has been added to the system, further decrease in the heights of density peaks of DPPC tails is observed. It is clear that adding protein to the system thickens the bilayer and makes the center deeper.

Figure S5 represents density profiles of four studied protein containing systems, simultaneously. Comparing Figures S5-C and S5-D clearly confirms the role of DMTAP lipids in increasing the bilayer thickness and the order of DPPC tails, which is accompanied by the lower area per lipid head groups.

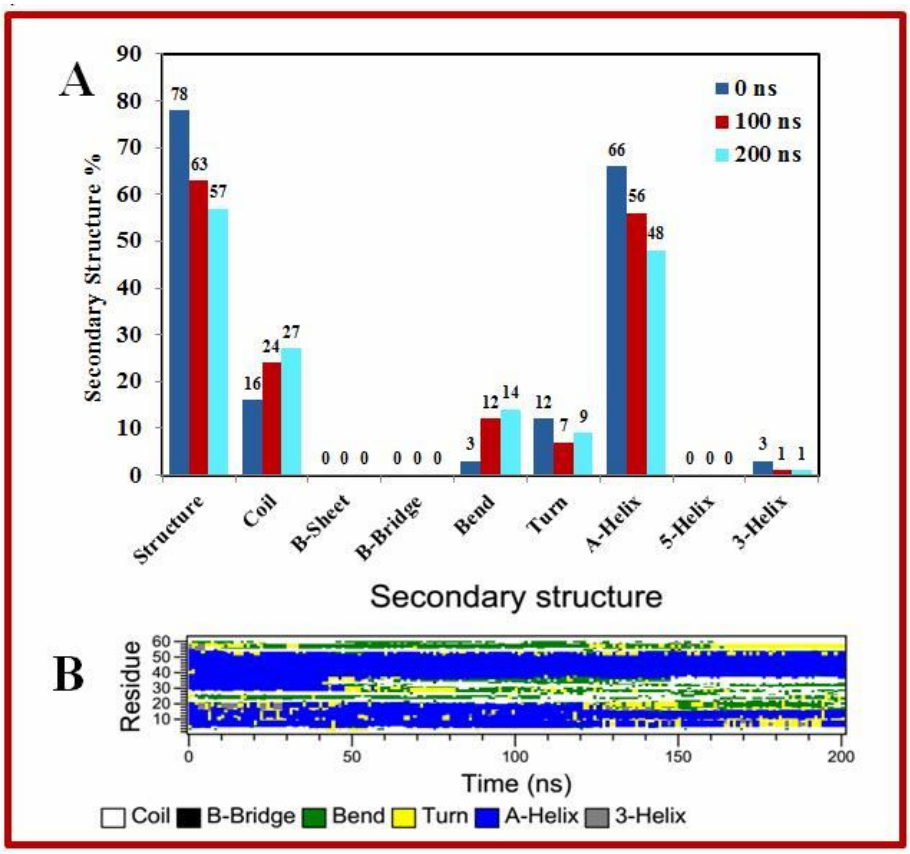

Fig. 7. Time evolution of secondary structural elements of TM23-GlyR in system 7, [DPPC60%-DMPC40% + TM23-GlyR] along the 200 ns MD simulation, generated by DSSP. The X-axis represents the molecular dynamics trajectory time (in ns), while the residue numbers are shown on the Y-axis.

Radius of Gyration

Radius of gyration (Rg) is defined as the mass weighted root mean square distance of a collection of atoms from their common center of mass. This property provides an insight into the overall dimensions of the protein, and so its compactness [64].

Figure S6 depicts the Rg plots of the TM23-GlyR membrane protein, along the 200 ns of simulation time for the four protein containing systems (5, 6, 7 and 8). Along with shedding light on the protein compactness, analysis of the Rg parameter is utilized to decide whether the protein structure has reached its equilibrium state or more simulation time is needed. As Fig. S6 illustrates, 200 ns is well enough simulation time for the protein molecule to find its equilibrium structure. In all systems (5, 6, 7 and 8), especially after half of the simulation time, the Rg parameter oscillates around its equilibrium value.

Comparison the Rg plots of systems 5 and 6 shows the effect of utilized lipid force filed on the compactness of TM23-GlyR protein. This transmembrane protein adopts more stable and compact structure in the vicinity of DPPC molecules, simulated using the GROMOS 43a1 force field. On the other hand, comparing the Rg plots of systems 5, [Pure DPPC (GROMOS 53A6) + TM23-GlyR] and 7, [DPPC60%-DMPC40% + TM23-GlyR], shows a little increase in the Rg value, due to replacing 40% of DPPC molecules with DMPC. As discussed earlier, based on the analysis of the structural properties of DPPC lipids, the presence of DMPC molecules leads to the lower order in the DPPC hydrocarbon chains, higher area per lipid, and

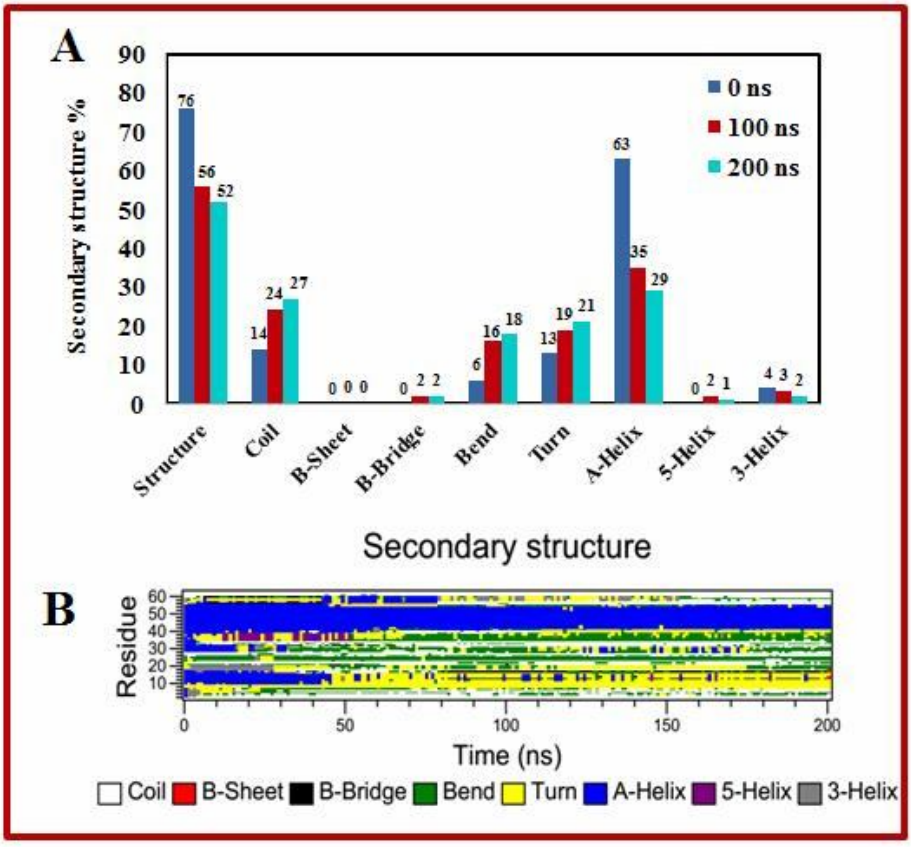

Fig. 8. Time evolution of secondary structural elements of TM23-GlyR in system 8, [DPPC60%-DMTAP40% + TM23-GlyR] along the 200 ns MD simulation, generated by DSSP. The X-axis represents the molecular dynamics trajectory time (in ns), while the residue numbers are shown on the Y-axis.

subsequently lower bilayer thickness. In spite of these obvious changes in the structural properties of DPPC molecules (after an insertion of 40% DMPC lipids), the Rg value of TM23-GlyR was not much affected.

When it comes to the systems 6 and 8, detectable decrease in the Rg value of the protein is observed in the latter system. This may be attributed to the special interactions between cationic DMTAP lipids and TM23-GlyR protein, also the role of DMTAP molecules on increasing the order and decreasing the area per lipid of the DPPC molecules. These effects altogether have led to the more compact structure of the TM23-GlyR transmembrane protein.

Hydrogen Bonding

Lipid tails, consisting of acyl chains, are hydrophobic and free of any charges, whereas head group regions of studied lipids, namely phosphatidylcholine in DPPC and DMPC, and trimethylammonium propane in DMTAP are zwitterionic and cationic, respectively. The polar head groups of each DPPC and DMPC molecules have eight possible hydrogen bond acceptors, while each DMTAP molecule has only four H-bond acceptors.

Figure S7 plots the number of hydrogen bonds of both DPPC and water molecules with the TM23-GlyR membrane protein in system 5, over the last 100 ns of the simulation time. DPPC lipids of this system give about15-19 hydrogen bonds with TM23-GlyR, during the considered simulation time, whereas protein molecule establishes more than 40 hydrogen bonds with the water molecules. As seen in Fig. S8, when 40% of DPPC lipids are substituted with DMPC, these two lipid kinds set up a comparable number of

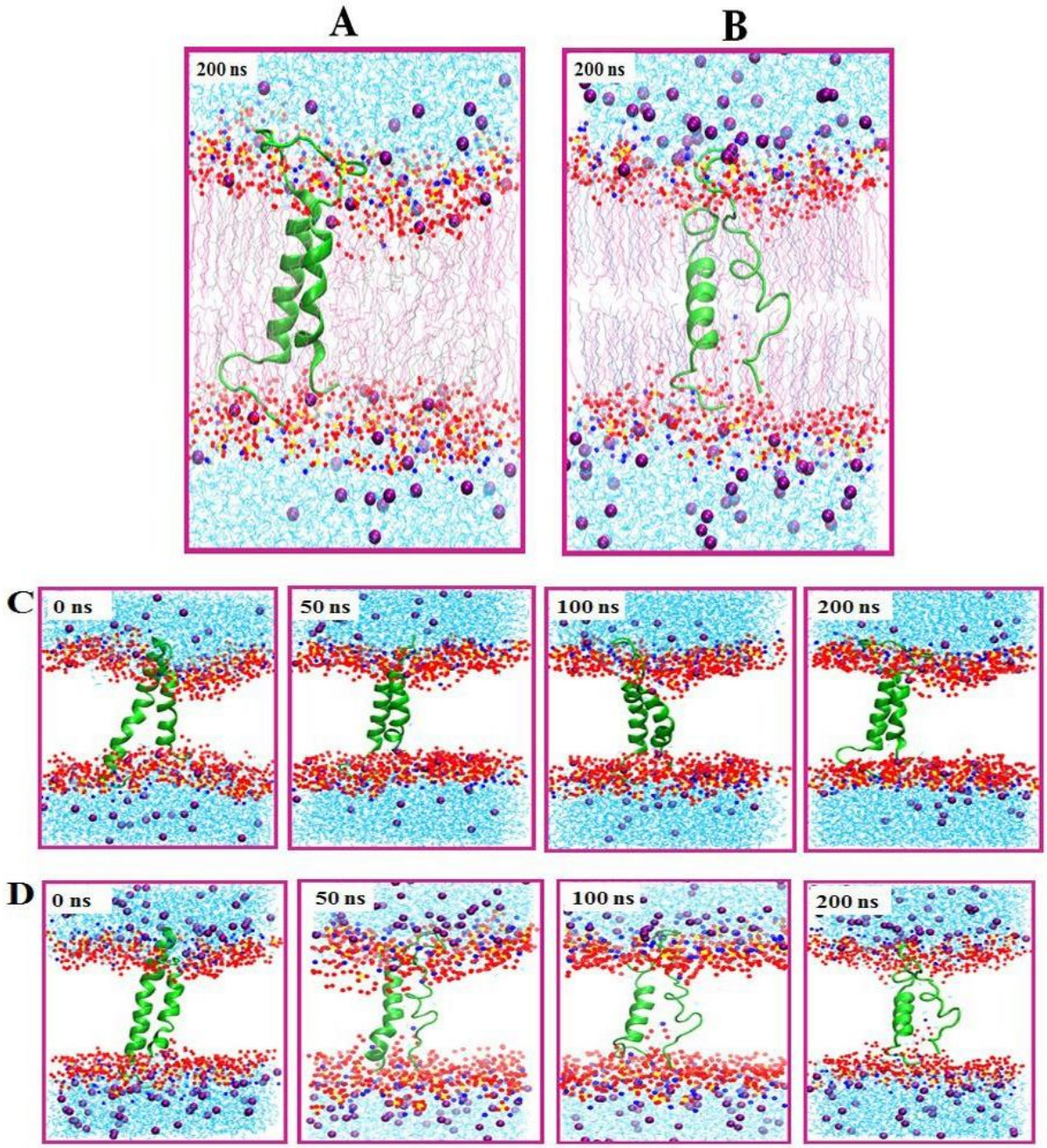

Fig. 9. Trajectory snapshots of A: system 7 (DPPC60%-DMPC40% + TM23-GlyR), and B: system 8 (DPPC60%-DMTAP40% + TM23-GlyR) at the end of simulation time. Parts C and D represent respectively the simulation boxes of systems 7 and 8 at different simulation times. TM23-GlyR is colored in green, while the phosphorus, oxygen and nitrogen atoms of DPPC in the bilayer are shown by yellow, red and blue points. Cyan line and purple spheres show the water molecules and ions, respectively. In parts A and B, the DPPC, DMPC and DMTAP lipids are colored in mauve, silver and iceblue, and in parts C and D, the lipid hydrocarbon chains were omitted for clarity.

hydrogen bonds (<10) with the protein molecule, while the number of hydrogen bonds between water molecules and the protein becomes higher in comparison to system 5.

When it comes to system 8, mutual interactions of zwitterionic DPPC and cationic DMTAP lipids with the protein molecule reduce the number of hydrogen bonds between the water molecules and protein to its lowest value compared to systems 5 and 7 (see Fig. S9). It seems that the local structural conformations of protein change in a way that it becomes more exposed to the lipid head groups for establishing hydrogen bonds. Further analysis of the TM23-GlyR secondary structure and also close inspection of the simulation box snapshots confirm this deduction.

Secondary Structure Analysis

In order to assess whether the mutual lipid-protein interactions induce any changes in the secondary structure of TM23-GlyR, DSSP program was employed. This program calculates the most likely secondary structure assignment, given the 3D structure of a protein. Figures 7 and 8 demonstrate the time evolution of secondary structural elements of TM23-GlyR along the 200 ns MD simulation in the systems 7, [DPPC60%-DMPC40% + TM23-GlyR], and 8, [DPPC60%-DMTAP40% + TM23-GlyR], respectively.

In both systems, fluctuations from helix to coil, turn, and bend structures are observed, while the residues 40-50 retain their α-helical structure. In the case of system 7, the main changes has been occurred in the secondary structural elements of residues 20-30 and 50-60, while system 8 has experienced structural changes in the residues 0-40 and 50-60. At the end of 200 ns MD simulation, the average α-helical content of systems 7 and 8 are 48% and 29%, respectively. These findings confirm that cationic DMTAP lipids have more potential to change the secondary structure of TM23-GlyR compared to the zwitterionic DMPC ones.

Trajectory Snapshots

Parts A and B of Fig. 9 represent respectively the simulation cells of systems 7 and 8, after 200 ns. In both systems, TM23-GlyR spans both the polar lipid head group, and the hydrophobic core of the lipid bilayer. Parts C and D of Fig. 9 show the extracted snapshots of simulation trajectories for systems 7 and 8 at four distinct simulation times (0, 50, 100 and 200 ns), where the lipid hydrocarbon chains are omitted to enhance the clarity. As mentioned in the previous section, the secondary structure of TM23-GlyR experiences more obvious changes in system 8 (compared to system 7), due to the presence of cationic DMTAP lipids. Snapshots of system 8 (Fig. 9-D), after 50 ns, support this finding, while further simulation time seems to unfold the protein completely.

The location, direction and secondary structure of the protein in the membrane surroundings are determined by the persistent hydrogen bonds between the donor atoms of the protein and the acceptors of the lipid head groups, and the weaker van der Waals interactions between the lipid acyl chains and the hydrophobic part of the protein. It is known that packing of transmembrane α-helices is dependent on the chain length of the surrounding phospholipids. In a broader view, physical influences affecting the membrane protein structure include interactions of the polypeptide chains with water, the bilayer hydrocarbon core, the bilayer interface, and even the ions present in the system.

In order to specify the main interactions between TM23-GlyR and the surrounding lipid head groups in system 8, Pymol program was employed. Fig. 10 depicts the dominant interactions of DPPC and DMTAP lipid head groups with the TM23-GlyR residues in system 8, at the end of 200 ns of MD simulation. Small boxes around the central box show the zoomed-in representations of the mutual lipid-protein interactions. As it is seen in Fig. 10, the protein residues Leu1, Ala3, Arg4, Thr17, Gln18, Arg23, Lys 28, Lys33, Val56, Asn57, Phe58, Ser60 and Arg61 participate mainly in the hydrogen bonding interactions with the lipid head groups.

CONCLUSIONS

This In-Silico study has employed the MD simulation approach to explore:

1) The mutual interactions of DMPC and DMTAP lipids with the DPPC molecules, and 2) The molecular-level interactions of the embedded TM23 part of the α-1 subunit of human glycine receptor (TM23-GlyR) with the pure DPPC, and the mixed DPPC-DMPC and DPPC-DMTAP bilayers. The all-atom MD simulations were carried out

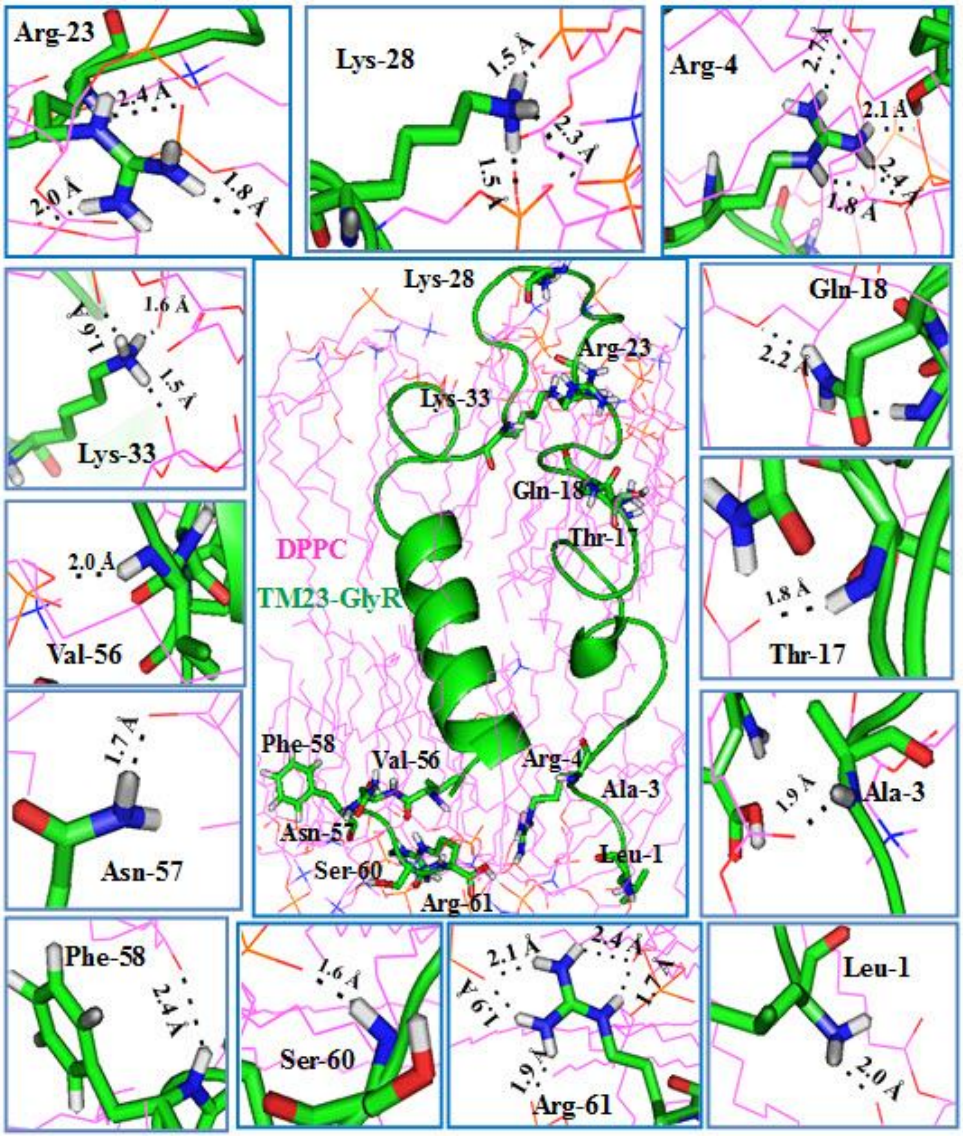

Fig. 10. Main interactions of lipid head groups with TM23-GlyR in system 8, [DPPC60%-DMTAP40% + TM23-GlyR].

using the Gromacs 5.4.1 simulation package, at 323 K under fully periodic boundary conditions.

The MD simulations of pure DPPC bilayer with the two different force fields, GROMOS 53a6 and GROMOS 43a1 (each for 10 ns), and analysis of RMSD, Box-x dimension, deuterium order parameter, area per lipid, average bilayer thickness and mass density profiles revealed the sensitivity of structure and dynamics of DPPC lipid bilayer to the changes in force field and simulation parameters. It should be noted that some bilayer properties like deuterium order parameter and area per lipid had more pronounced force filed dependence, while others like mass density profile were less sensitive.

In the next step, mixed (DPPC60%-DMPC40%) and (DPPC60%-DMTAP40%) bilayers were each simulated for 10 ns, and the effect of added lipids on the structural and dynamical properties of DPPC molecules were analyzed in detail.

The lower deuterium order parameter values for both *sn*-1 and *sn*-2 chains of DPPC molecules, in (DPPC60%-DMPC40%) bilayer, compared to the pure DPPC system, was a clear indication of order loss. This observation was attributed to the difference in the hydrocarbon chain lengths of DPPC and DMPC molecules, which forces the DPPC lipids to shorten their hydrophobic tails, in order to establish more effective non-polar interactions with hydrocarbon tails of DMPC molecules. Adding 40% of DMPC lipids to the pure DPPC bilayer also led to the decrease in the bilayer thickness, along with increase in the area per lipid head groups.

On the other hand, adding cationic DMTAP lipids to the pure DPPC bilayer resulted in more tangible effects on the structural properties of DPPC molecules. This is due to the cationic nature of DMTAP lipids enabling them to establish strong electrostatic interactions with the zwitterionic head groups of DPPC molecules. Putting together 40% of DMTAP and 60% of DPPC lipid molecules gave rise an increase in the order of DPPC acyl chains and the bilayer thickness, accompanied by decreasing the area per lipid head groups.

Finally, the g_membed tool was employed in order to insert the TM23-GlyR into the pure and mixed bilayers, and the resulting four protein containing systems were simulated each for 200 ns. The bilayer insertion of TM23-GlyR led to an obvious increase in the long range order of DPPC lipid chains, confirmed by analyzing the radial distribution plots, while this impact was more profound in DMTAP containing mixed lipid bilayer.

The significant increase in deuterium order parameters of DPPC tails in (DPPC60%-DMTAP40% + TM23-GlyR) system supported the role of mutual lipid-protein interactions in increasing the configurational order of lipid chains, which in turn is an indication of the positive hydrophobic mismatch. Higher bilayer thickness around the box center, where TM23-GlyR was inserted, supported this conclusion.

On the other hand, analysis of protein's structural properties, conveyed that positively charged DMTAP lipids have more potential to change the secondary structure of TM23-GlyR compared to the zwitterionic DMPC ones. In fact, the local structural features of the protein are changed in a way that they become more exposed to the lipid head groups for establishing the stabilizing hydrogen bonds. As an example, the hydrogen bonding network of DPPC and DMTAP lipid head groups with the TM23-GlyR residues were analyzed and illustrated schematically for the (DPPC60%-DMTAP40% + TM23-GlyR) system. This study with the detailed molecular level analysis of lipid protein interactions could shed light on the effect of lipid force field, chain length, and the head group charge and size, on the configurational, structural and dynamical properties of both lipid and protein molecules.

ACKNOWLEDGEMENTS

The authors gratefully acknowledge the Shiraz University of Technology for providing the computational resources for this project.

REFERENCES

[1] Breitinger, H. G.; Glycine Receptors, In: eLS. John Wiley & Sons Ltd., Chichester, 2014.

[2] Tang, B.; Lummis, S. C. R., Multiple regions in the extracellular domain of the glycine receptor determine receptor activity, *J. Biol. Chem.* **2018**, *293*, 13889-13896, DOI: 10.1074/jbc.RA118.003088.

[3] Lynch, J. W., Molecular structure and function of the glycine receptor chloride channel, *Physiol. Rev.* **2004**, *84*, 1051-1095, DOI: 10.1152/physrev.00042.2003.

[4] Miyazawa, A.; Fujiyoshi, Y.; Unwin, N., Structure and gating mechanism of the acetylcholine receptor pore, *Nature*, **2003**, *423*, 949-55, https://www.nature.com/articles/nature01748.

[5] Bechade, C.; Sur, C.; Triller, A., The inhibitory neuronal glycine receptor, *BIOESSAYS,* **1994**, *16*, 735-744, DOI:10.1002/bies.950161008.

[6] Cheng, M. H.; Coalson, R. D.; Casico, M.; Kurnikova, M., Computational prediction of ion permeation characteristics in the glycine receptor modified by photo-sensitive compounds, *J. Comput. Aided Mol. Des.* **2008**, *22*, 563-570, DOI: 10.1007/s10822-008-9200-0.

[7] Taleb, O.; Betz, H., Expression of the human glycine receptor a 1 subunit in Xenopus oocytes: apparent affinities of agonists increase at high receptor density,

EMBO J. **1994**, *13*, 1318-1324, DOI: 10.1002/j.1460-2075.1994.tb06384.x.

[8] Deol, S. S.; Bond, P. J.; Domene, C.; Sansom, M. S. P., Lipid-protein interactions of integral membrane proteins: A comparative Simulation study, *Biophys. J.* **2004**, *87*, 3737-3749, DOI: 10.1529/ biophysj.104.048397.

[9] Arnaud, C. H., Chemical and Engineering News, 2017, Vol. 95, pp. 18-20.

[10] Pogozheva, I. D.; Mosberg, H. I.; Lomize, A. L., Life at the border: Adaptation of proteins to anisotropic membrane environment, *Protein Sci.* **2014**, *23*, 1165-1196, DOI:10.1002/pro.2508.

[11] Marothy, M. T.; De Elofsson, A., Marginally hydrophobic transmembrane a-helices shaping membrane protein folding, *Protein Sci.,* **2015**, *24*, 1057-1074, DOI: 10.1002/pro.2698.

[12] Jensen, M. Ø.; Mouritsen, O. G.; Peters, G. H., Simulations of a membrane-anchored peptide: structure, dynamics, and influence on bilayer properties, *Biophys J.* **2004**, *86*, 3556-3575, DOI: 10.1002/pro.2698.

[13] Berne`che, S.; Nina, M.; Roux, B., Molecular dynamics simulation of melittin in a dimyristoylphosphatidylcholine bilayer membrane, *Biophys. J.*, **1998**, 75, 1603-1618, DOI: 10.1016/ S0006-3495(98)77604-0.

[14] Kandasamy, S. K.; Larson, R. G., Molecular dynamics simulations of model trans-membrane peptides in lipid bilayers: A systematic investigation of hydrophobic mismatch, *Biophys. J.,* **2006**, *90*, 2326-2343, DOI:10.1529/biophysj.105.073395.

[15] Nagle, J. F.; Tristram-Nagle, S., Structure of lipid bilayers, *Biochim. Biophys. Acta,* **2000**, *1469* 159-195, DOI: 10.1016/S0304-4157(00)00016-2.

[16] Rheinstadter, M. C.; Seydel, T.; Demmel, F.; Salditt, T., Molecular motions in lipid bilayers studied by the neutron backscattering technique, *Phys. Rev. E,* **2005**, *71*, 061908. DOI: 10.1103/PhysRevE.71.061908.

[17] Binder, H.; Water near lipid membranes as seen by infrared spectroscopy. *Eur. Biophys. J.* **2007**, *36*, 265-279, DOI: 10.1007/s00249-006-0110-6.

[18] Zhou, Z.; Sayer, B. G.; Hughes, D. W.; Stark, R. E.; Epand, R. M., Studies of phospholipid hydration by high-resolution magic-angle spinning nuclear magnetic resonance, *Biophys. J.* **1999**, *76*, 387-399, DOI: 10.1016/S0006-3495(99)77205-X.

[19] Drew Bennett, W. F.; Peter Tieleman, D., Computer simulations of lipid membrane domains, *Biochim. Biophys. Acta.* **2013**, *1828*, 1765-1776. DOI: 10.1016/j.bbamem.2013.03.004.

[20] Strandberg, E.; Morein, S.; Rijkers, D. T. S.; Liskamp, R. M. J.; van der Wel, P. C. A.; Killian, J. A., Lipid dependence of membrane anchoring properties and snorkeling behavior of aromatic and charged residues in transmembrane peptides, *Biochemistry,* **2002**, *41*, 7190-7198. DOI: 10.1021/bi012047i.

[21] Bystrom, T.; Grobner, G.; Lindblom, G., Orientation of a polyleucine-based peptide in phosphatidy1choline bilayers of different thickness, Solid-state NMR and CD spectroscopy, *Colloids Surf. A Physicochem. Eng. Asp*. **2003**, *228*, 37-42, DOI: 10.1016/S0927-7757(03)00303-0.

[22] Mohammad-Aghaie, D.; Mace, E.; Sennoga, C. A.; Seddon, J. M.; Bresme, F., Molecular dynamics simulations of liquid condensed to liquid expanded transitions in DPPC monolayers, *J. Phys. Chem. B,* **2010**, *114*, 1325-1335. DOI: 10.1021/jp9061303.

[23] Berger, O.; Edholm, O.; Jahnig, F., Molecular dynamics simulations of a fluid bilayer of dipalmitoylphosphatidylcholine at full hydration, constant pressure, and constant temperature, *Biophys. J.* **1997**, *72*, 2002-2013, DOI: 10.1016/S0006-3495(97)78845-3.

[24] Mohammad-Aghaie, D.; Bresme, F., Force-field dependence on the liquid-expanded to liquid-condensed transition in DPPC monolayers, *Mol. Simul.* **2016**, *42*, 391-397, DOI: 10.1080/ 08927022.2015.1059428.

[25] Kandt, Ch.; Mátyus, E.; Tieleman, D. P., Protein Lipid Interactions from a Molecular Dynamics Simulation Point of View, in: Structure and Dynamics of Membranous Interfaces, Chapter 10, 2008, p. 267-282. DOI: 10.1002/9780470388495.ch10.

[26] Bachar, M.; Becker, O. M., Protein-induced membrane disorder: A molecular dynamics study of melittin in a dipalmitoylphosphatidylcholine bilayer, *Biophys. J.* **2000**, *78*, 1359-1375, DOI: 10.1016/

S0006-3495(00)76690-2.

[27] Lee, A. G., How lipids affect the activities of integral membrane proteins, *Biochim. Biophys. Acta,* **2004**, *1666*, 62-87, DOI: 10.1016/ j.bbamem.2004.05.012.62–87.

[28] Kandasamy, S. K.; Larson, R. G., Molecular dynamics study of the lung surfactant peptide SP-B with DPPC monolayers: Insights into interactions and peptide position and orientation, *Biophys. J.* **2005**, *88*, 1577-1592. DOI:10.1529/biophysj.104.038430.

[29] Cheng, M. H.; Xu, Y.; Tang, P., Anionic lipid and cholesterol interactions with a4ß2 nAChR: Insights from MD simulations, *J Phys Chem B.,* **2009**, *113*, 6964-6970, DOI: 10.1021/jp900714b.

[30] Wang, Y.; Schlamadinger, D. E.; Kim, J. E.; McCammon, J. A., Comparative molecular dynamics simulations of the antimicrobial peptide CM15 in model lipid bilayers, *Biochim. Biophys. Acta.* **2012**, *1818*, 1402-1409, DOI: 10.1016/ j.bbamem.2012.02.017.

[31] Lockhart, C.; Klimov, D. K., Binding of Aß peptide creates lipid density depression in DMPC bilayer, *Biochim. Biophys. Acta,* **2014**, *1838*, 2678-2688, DOI: 10.1016/j.bbamem.2014.07.010.

[32] Duan, X.; Li, Y.; Zhang, R.; Shi, T.; An L.; Huang, Q., Regulation of anionic lipids in binary membrane upon the adsorption of polyelectrolyte: A Monte Carlo simulation, *AIP Adv.,* **2013**, *3*, 062128, DOI:10.1063/1.4812699.

[33] Yamamoto, E., Computational and theoretical approaches for studies of a lipid recognition protein on biological membranes, *Biophys. Physicobiol.,* **2017**, *14*, 153-160, DOI: 10.2142/ biophysico.14.0_153.

[34] Khalid, S.; Bond, P. J.; Holyoake, J.; Hawtin, R. W.; Sansom, M. S. P., DNA and lipid bilayers: Self-assembly and insertion, *J. R. Soc. Interface,* **2008**, *5*, S241-S250, DOI: 10.1098/rsif.2008.0239.focus.

[35] Gurtovenko, A. A.; Patra, M.; Karttunen, M.; Vattulainen, I., Cationic DMPC/DMTAP lipid bilayers: Molecular dynamics study, *Biophys. J.* **2004**, *86*, 3461-3472, DOI: 10.1529/biophysj.103.038760.

[36] Zhi, D.; Bai, Y.; Yang, J.; Cui, Sh.; Zhao, Y.; Chen, H.; Zhang, S., A review on cationic lipids with different linkers for gene delivery, *Adv Colloid Interface Sci.* **2018**, *253*, 117-140, DOI: 10.1016/ j.cis.2017.12.006.

[37] Ma, D.; Liu, Z.; Li, L.; Tang, P.; Xu, Y., Structure and dynamics of the second and third transmembrane domains of human glycine receptor, *Biochemistry,* **2005**, *44*, 8790-8800, DOI: 10.1021/bi050256n.

[38] Abraham, M. J.; Murtola, T.; Schulz, R.; Pall, S.; Smith, J. C.; Hess, B.; Lindahl E., GROMACS: High performance molecular simulations through multi-level parallelism from laptops to supercomputers, *SoftwareX,* **2015**, *1-2*, 19-25, DOI: 10.1016/ j.softx.2015.06.001.

[39] Li, J.; Wang, X.; Zhang, T.; Wang, Ch.; Huang, Zh.; Luo, X.; Deng, Y., A review on phospholipids and their main applications in drug delivery systems, *Asian J. Pharm. Sci.* **2015**, *10*, 81-98. DOI: 10.1016/j.ajps.2014.09.004.

[40] Ghahremanpour, M. M.; Arab, S. Sh.; Biook Aghazadeh, S.; Zhang, J.; Van der Spoel, D., MemBuilder: a web-based graphical interface to build heterogeneously mixed membrane bilayers for the GROMACS biomolecular simulation program, *Bioinformatics,* **2014**, *30*, 439-441, DOI: 10.1093/ bioinformatics/btt680.

[41] Lomize, M. A.; Pogozheva, I. D.; Joo, H.; Mosberg, HI.; Lomize, A. L., OPM database and PPM web server: resources for positioning of proteins in membranes, *Nucleic Acids Res.* **2012**, *40*, D370-D376, DOI: 10.1093/nar/gkr703.

[42] Wolf, M. G.; Hoefling, M.; Aponte-Santamar´ia, C.; Grubm¨uller, H.; Groenhof, G., g_membed: Efficient insertion of a membrane protein into an equilibrated lipid bilayer with minimal perturbation, *J. Comput. Chem.* **2010**, *31*, 2169-2174, DOI: 10.1002/jcc.21507.

[43] Ryckaert, J. -.P.; Bellemans, A., Molecular dynamics of liquid n-butane near its boiling point, *Chem. Phys. Lett.* **1975**, *30*, 123-125, DOI: 10.1016/0009-2614(75)85513-8.

[44] Ryckaert, J. -P.; Bellemans, A., Molecular dynamics of liquid alkanes, Faraday Discuss. *Chem. Soc.* **1978**, *66*, 95-106, DOI: 10.1039/DC9786600095.

[45] Chiu, S. W.; Clark, M.; Balaji, V.; Subramaniam, S.; Scott, H. L.; Jakobsson, E., Incorporation of surface

tension into molecular dynamics simulation of an interface: a fluid phase lipid bilayer membrane, *Biophys. J.,* **1995**, *69*, 1230-1245, DOI: 10.1016/S0006-3495(95)80005-6.

[46] Lemkul**,** J. A.; From proteins to perturbed hamiltonians: A suite of tutorials for the GROMACS-2018 molecular simulation package, *Living J. Comp. Mol. Sci.,* **2018**, *1*, 1-53, DOI : 10.33011/ livecoms.1.1.5068.

[47] Hirshman, S. P.; Whitson, J. C., Steepest-descent moment method for three-dimensional magnetohydrodynamic equilibria, *J. C. Phys. Fluids,* **1983**, *26*, 3553-3568, DOI: 10.1063/1.864116.

[48] Parrinello, M.; Rahman A., Polymorphic transitions in single crystals: A new molecular dynamics method, *J. Appl. Phys.* **1981**, *52*, 7182, DOI:10.1063/1.328693.

[49] Essmann, U.; Perera, L.; Berkowitz, M. L.; Darden, T.; Lee, H.; Pedersen, L. G., A smooth particle mesh ewald method, *J. Chem. Phys.* **1995**, *103*, 8577-8593, DOI: 10.1063/1.470117.

[50] Humphrey, W.; Dalke, A.; Schulten, K., VMD: Visual molecular dynamics*, J. Mol. Graphics,* **1996**, *14*, 33-38, DOI: 10.1016/0263-7855(96)00018-5.

[51] DeLano, W. L., The PyMOL Molecular Graphics System, Version 1.8 Schrödinger, LLC. Delano Scientific, San Carlos.

[52] Duncan, S. L.; Dalal, I. S.; Larson, R. G., Molecular dynamics simulation of phase transitions in model lung surfactant monolayers, *Biochim Biophys Acta,* **2011**, *1808*, 2450-2465, DOI: 10.1016/ j.bbamem.2011.06.026.

[53] Piggot, T. J.; Allison, J. R.; Sessions, R. B.; Essex, J. W., On the calculation of acyl chain order parameters from lipid simulations, *J. Chem. Theory Comput.* **2017**, *13*, 5683-5696, DOI: 10.1021/acs.jctc.7b00643.

[54] Leekumjorn, S.; Sum, A. K., Molecular simulation study of structural and dynamic propertiesof mixed DPPC/DPPE *Bilayers, Biophys. J.* **2006**, *90,* 3951-3965, DOI: 10.1529/biophysj.105.076596.

[55] Thomas, J., Biomedical applications of biophysics, Humana Press, Totowa, NJ, 2010, DOI: 10.1007/978-1-60327-233-9.

[56] Berkowitz, M. L.; Vacha, R., Aqueous solutions at the interface with phospholipid bilayers, *Acc. Chem. Res.* **2012**, 45, 74-82, DOI: 10.1021/ar200079x.

[57] Allen, W. J.; Lemkul, J. A.; Bevan, D. R., GridMAT-MD: A grid-based membrane analysis tool for use with molecular dynamics, *J. Comput. Chem.* **2009**, *30*, 1952-1958, DOI: 10.1002/jcc.21172.

[58] Poger, D.; Mark, A. E., Lipid bilayers: The effect of force field on ordering and dynamics, *J. Chem. Theory Comput.* **2012**, *8*, 4807-4817, DOI: 10.1021/ ct300675z.

[59] Andersen, O. S.; Koeppe, R. E., Bilayer thickness and membrane protein function: An energetic perspective, *Annu. Rev. Biophys. Biomol. Struct.,* **2007**, *36*, 107-130, DOI: 10.1146/ annurev.biophys.36.040306.132643.

[60] Lemkul, J. A.; Bevan, D. R., Perturbation of membranes by the amyloidb-peptide -a molecular dynamics study, *FEBS Journal,* **2009**, *276*, 3060-3075, DOI: 10.1111/j.1742-4658.2009.07024.x.

[61] Kučerka, N.; Nieh, M. P.; Katsaras, J., Fluid phase lipid areas and bilayer thicknesses of commonly used phosphatidylcholines as a function of temperature, *Biochim Biophys Acta,* **2011**, *1808*, 2761-2771, DOI: 10.1016/j.bbamem.2011.07.022.

[62] Edler, E.; Schulze, E.; Stein, M., Membrane localization and dynamics of geranylgeranylated Rab5 hypervariable region, *Biochim Biophys Acta,* **2017**, *1859*, 1335-1349, DOI: 10.1016/ j.bbamem.2017.04.021.

[63] Moradi, S.; Nowroozi, A.; Shahlaei, M., Shedding light on the structural properties of lipid bilayers using molecular dynamics simulation: a review study, *RSC Adv.,* **2019**, *9*, 4644-4658, DOI: 10.1039/ C8RA08441F.

[64] Baig, M. H.; Sudhakar, D. R.; Kalaiarasan, P.; Subbarao, N.; Wadhawa, G.; Lohani, M.; Khan, M. K. A.; Khan, A. U., Insight into the effect of inhibitor resistant S130G mutant on physico-chemical properties of SHV type beta-lactamase: A molecular dynamics study, *PLoS One.* **2014**, *9*, e112456, DOI: 10.1371/journal.pone.0112456.